Visualization of molecular flexibility and its effects on electrostatic recognition

Cindy L. Fisher, John A. Tainer, Michael E. Pique, and Elizabeth D. Getzoff

Department of Molecular Biology, Research Institute of Scripps Clinic, La Jolla, CA, USA

To study the effect of protein flexibility on electrostatic recognition, we have devised two novel computer graphic representations of the changes in the electrostatic field of a protein resulting from its internal motions. The atomic structure of Cu, Zn superoxide dismutase was minimized, and the 200 lowest frequency normal modes of the enzyme were determined. Individual and combined normal-mode vibrations were visualized interactively with the program Flex. *Normal-mode motions are fast enough ($\sim 10^{-11}$ s cycle^{-1}) to evade solvent damping, thus allowing long-range electrostatic interactions to dominate. The changing electrostatic environment of the protein was examined by animating precalculated frames of electrostatic field vectors with* GRAMPS. *With* Vu, *changes in electrostatic potential were displayed as variations in the color-coding of dots lying on a consensus surface that maintains the protein's shape. The consensus surface was calculated with the program* Sphinx, *and was derived from spherical harmonic approximations of expanded molecular surfaces. The ability to view the effects of molecular motions interactively should be useful in understanding the relationships of protein structure to function.*

Keywords: normal modes, computer graphics, molecular surface, protein structure, superoxide dismutase

INTRODUCTION

Electrostatic recognition plays an important role in protein function. Through rate enhancement and orientation effects, charge interactions guide many protein associations, including enzyme–substrate reactions, electron and proton transfers, and subunit–subunit interactions.

Generally, theoretical studies of global electrostatic recognition involve a static picture of the protein, typically taking atomic coordinates from x-ray diffraction studies as the basis for calculation. The role of electrostatic forces has been examined in biologically important macromolecular interactions,[1] involving the families of cytochromes,[2–11] globins,[12] proteases,[13–15] nucleic acid binding proteins,[16,17] and many others,[18] usually with stationary protein models. The incoming substrate, however, does not see a stationary protein. Both global and local motion may affect the electherefore introduce in this work two computer graphics methods for observing the behavior of the electrostatic environment around a moving protein.

To address the effects of molecular motion on protein reactions and interactions, which occur on time scales of 10^{-10} to 10^{3} or more seconds,[19] theoretical calculations must model motions occurring on similar time scales.[1,20,21] With present computational capabilities, molecular dynamics techniques can be used to study local electrostatic behavior,[3,20,22] once the interacting molecules are positioned by rigid body movements, but cannot practically examine global macromolecular behaviors and long-distance electrostatic recognition occurring on slower time scales.[20] The two most computationally accessible methods for calculating interactions with longer time scales are normal-mode analysis and Brownian dynamics. In this work, normal-mode calculations are used to obtain snapshots of protein motion, which are analyzed with molecular graphical representations of the dynamic electrostatic fields. Each normal mode corresponds to a characteristic vibration at a given frequency generated from the potential and kinetic energy of the protein, ranging from 10^{-11} to 10^{-14} s cycle^{-1}, with longer time scales accessible through periodic repetition.

The protein we have chosen as a developmental model is the enzyme copper, zinc superoxide dismutase (Cu,Zn SOD; EC 1.15.1.1). SOD, which is found in all aerobic organisms, catalyzes the dismutation of superoxide radical to hydrogen peroxide and molecular oxygen.[23,24] Cu,Zn SOD, found primarily in eucaryotic organisms, contains at the bottom of a deep active site channel[25] a copper ion that is alternately reduced and oxidized in the dismutation process.[26] A fascinating aspect of the mechanism of this protein, as evidenced by ionic strength studies,[27,28] is the electrostatic guidance to the copper ion afforded to the incoming superoxide anion by the high concentration of positively charged amino acid residues around the active site.[29] The electrostatic assistance supplied by the concentrated positive field is a major factor in the rapid catalytic rate of the enzyme (2×10^{9} M^{-1} s^{-1}, or about 5×10^{-10} s for each reaction),[30] which exceeds the expected unfacilitated

Address reprint requests to Dr. Getzoff at the Department of Molecular Biology, Research Institute of Scripps Clinic, La Jolla, CA 92037, USA.
Received 5 December 1989; accepted 19 April 1990

diffusion rate given the steric constraints of the copper ion when surrounded by the protein. Thus, SOD provides an excellent system for testing electrostatic modeling.

Several researchers have developed stationary models of SOD electrostatics using the published crystal structure.[31,32] The initial work on SOD calculated the electrostatic potential around the active site using a simple Coulombic relationship.[29] The direction of the electrostatic field was represented by arrows, color-coded according to the electrostatic potential. Another approach involved building a grid around the protein and approximating the electrostatic potential at each grid point from the Poisson–Boltzmann equation.[33,34] The resultant potential was depicted as isopotential contours around the protein.[33] Yet another method, also utilizing Poisson–Boltzmann approximations, modeled the protein as a sphere[35–37] or as point charges on a grid[34,38–40] to carry out Brownian dynamics simulations of superoxide diffusion.

To determine whether a moving representation of the enzyme would extend the electrostatic field over a wider area around the active site, we have conducted a normal-mode analysis of SOD, where the time scales of movement are about 10^{-12}–10^{-11} s (about 10–100 times per reaction of SOD with superoxide). From these results, a major goal of this work was achieved—to devise computer graphical representations of the changes in the electrostatic field of a protein in motion.

THEORETICAL METHODS

For the development of the visualization approaches reported here, normal-mode calculations were limited in size by using only one of the two SOD subunits of the active dimer found in vivo. Since the active sites lie on opposite sides of the dimer, i.e., far from the dimer interface, this approximation is a reasonable initial model. We used the reported x-ray diffraction coordinates of the first SOD subunit,[25] including polar hydrogen atoms and seven water molecules in the active site channel, for a total of 1369 atoms. The coordinates were energy-minimized with the program AMBER[41] using a united atom approximation (only heavy atoms and polar hydrogens included; nonpolar hydrogen atoms were merged with the parent carbon atom) until the maximum derivative in energy was less than 1×10^{-3} kcal mol^{-1} Å^{-1}. AMBER uses the force field equation:

$$E_{\text{total}} = \sum_{\text{bonds}} K_r(r - r_{\text{eq}})^2 + \sum_{\text{angles}} K_\theta(\theta - \theta_{\text{eq}})^2 + \sum_{\text{dihedrals}} \frac{V_n}{2}[1 + \cos(n\phi - \gamma)] + \sum_{i<j} \left(\frac{A_{ij}}{R_{ij}^{12}} - \frac{B_{ij}}{R_{ij}^{6}} + \frac{q_i q_j}{\epsilon R_{ij}}\right) + \sum_{\text{H bonds}} \left(\frac{C_{ij}}{R_{ij}^{12}} - \frac{D_{ij}}{R_{ij}^{10}}\right) \quad (1)$$

to define the potential energy required to deform each of the internal coordinates from their standard, unstrained state (indicated by the variables r_{eq}, θ_{eq}, and the phase γ). The parameters K_r, K_θ, and $V_n/2$ are the force constants for the intramolecular deformations of bond lengths, bond angles, and dihedral angles, respectively. The general nonbonded repulsive and dispersive interactions are represented by a 6–12 Lennard–Jones potential (with parameters A_{ij} and B_{ij}, related to the van der Waals radius and well depth), while hydrogen-bonding interactions are represented by a 10–12 potential (with parameters C_{ij} and D_{ij}). The electrostatic interactions are defined with a distance-dependent Coulombic relationship. Published potential energy parameters[41,42] were used except for the following modifications to accommodate the copper and zinc ions. For the metal-ligating residues—His 44, His 46, His 61, and His 118 for the copper and His 61, His 69, His 78, and Asp 81 for the zinc—weak bond and angle forces were added to represent metal–ligand coordination, and partial charges were adjusted to more realistically represent delocalization of the formal metal ion charges onto the ligands. Values for equilibrium bond lengths (r_{eq}) and bond angles (θ_{eq}; see Table 1) were taken from average values in the Cambridge Structural Data Base for small-molecule crystal structures that contain copper or zinc and appropriate ligands. All bonds involving the two metal ions had $K_r = 80$ kcal mol^{-1} Å^{-2}, a weak force constant compared to, for example, C–C bonds that have K_r from about 200 to 550 kcal mol^{-1} Å^{-2}. Copper–nitrogen, zinc–nitrogen, and zinc–oxygen bonds were assigned r_{eq} values of 2.06, 2.04, and 1.97 Å, respectively. The ligand–metal–ligand angles were given a weak force constant of 30 kcal mol^{-1} for K_θ. For all torsion angles involving the copper or zinc ions, the value of $V_n/2$ was set to 0.0 kcal mol^{-1}, negating any torsional contributions to the energy. The nonbond parameters A_{ij} and B_{ij} were set to 0.45 kcal mol^{-1} Å^{-12} and 0.30 kcal mol^{-1} Å^{-6} (assuming a somewhat weak contribution to the van der Waals energy) for both copper and zinc. The partial charges (Table 2) were derived by placing a charge of +0.5 on each of the two metals and distributing the remaining +1.5 charge on each

Table 1. Angle parameters for SOD active site

Angle[a]	θ_{eq}
CU–NA–CG	126.0
CU–NA–CP	126.0
CU–NB–CP	126.0
CU–NB–CC	126.0
NA–CU–NB	111.0
NB–CU–NB	111.0
CF–NB–CU	126.0
NA–ZN–NB	115.0
NB–ZN–NB	115.0
NA–ZN–O2	103.0
NB–ZN–O2	103.0
CP–NA–ZN	127.0
CG–NA–ZN	127.0
CP–NB–ZN	127.0
CC–NA–ZN	127.0
CC–NB–ZN	127.0
ZN–O2–C	116.0

[a] AMBER nomenclature used for atom types

Table 2. Partial charge parameters for SOD active site

Residue	Atom	Charge	Standard[a]	Residue	Atom	Charge	Standard[a]
HIS1[b]	N	−0.520	−0.520	ASP1[d]	N	−0.520	−0.520
	HN	0.248	0.248		HN	0.248	0.248
	CA	0.219	0.219		CA	0.206	0.246
	CB	0.027	0.060		CB	−0.105	−0.208
	CG	0.160	0.112		CG	0.420	0.620
	ND1	−0.320	−0.527		OD1	−0.450	−0.706
	CE1	0.455	0.384		OD2	−0.450	−0.706
	NE2	−0.400	−0.444		C	0.526	0.526
	HNE	0.280	0.320		O	−0.500	−0.500
	CD2	0.200	0.122				
	C	0.526	0.526				
	O	−0.500	−0.500				
	Total	0.375	0.000		Total	−0.625	−1.000
HIS2[c]	N	−0.520	−0.520	HICZ[e]	N	−0.520	
	HN	0.248	0.248		HN	0.248	
	CA	0.219	0.219		CA	0.219	
	CB	0.027	0.060		CB	0.027	
	CG	0.160	0.089		CG	0.220	
	ND1	−0.400	−0.444		ND1	−0.550	
	HND	0.280	0.320		ZN	0.500	
	CE1	0.455	0.384		CE1	0.370	
	NE2	−0.320	−0.527		NE2	−0.550	
	CD2	0.200	0.145		CU	0.500	
	C	0.526	0.526		CD2	0.260	
	O	−0.500	−0.500		C	0.526	
					O	−0.500	
	Total	0.375	0.000		Total	0.750	

[a] Standard AMBER charges for the equivalent residue type
[b] Used for neutral histidines bonded to metal ion through the δ nitrogen (44, 69, and 78)
[c] Used for neutral histidines bonded to metal ion through the ϵ nitrogen (46 and 118)
[d] Used for metal-ligating aspartate (81)
[e] Used for the negatively charged histidine bridging copper and zinc (61)

metal equally among its ligands. To match the active site geometry determined crystallographically,[25] the new residue type HIS1 was used for His 44, 69, and 78, which are bonded to the metal ion through their δ nitrogens, and HIS2 was used for His 46 and 118, which are bonded to the metal ion through their ϵ nitrogens. HICZ was used for His 61, the histidine that bridges the copper and zinc, and ASP1 was used for Asp 81. The final minimized structure had an RMS deviation from the original x-ray coordinates of 1.54 Å for all heavy atoms (1.14 Å for Cα atoms, 0.60 Å for the crystallographically well-ordered heavy atoms of the active site residues and metal ions).

For normal-mode analysis, the protein was treated as a system of multiple harmonic oscillators consisting of point masses (atoms) connected with harmonically oscillating springs (bonds) that vibrate about the energy minimum. Normal modes were calculated by solving for the eigenvalues of the mass-weighted force constant matrix $\mathbf{F}$, where $\mathbf{F} = \mathbf{M}^{-1/2}\nabla^2 E$ ($\mathbf{M}$ is the diagonal matrix of the atomic masses and E is the potential energy). The 200 lowest-frequency normal modes of the SOD subunit were determined from the minimized structure with the local version of AMBER reparametrized to handle vibrational analysis for systems this large. The program generated a file containing the absolute vibrational displacements for each atom at each frequency. The normal modes exhibiting the largest displacements in residues around the rim of the active site channel were selected, including those predicted to dominate the electrostatic steering.[29] Each selected mode was studied independently and in combination with other modes with the program Flex (described below) in order to characterize the motions. Selected modes were examined further. A series of five displacements were generated: the nondisplaced, energy-minimized coordinates about which the motion is centered, the maximum positive and negative displacements, assuming a temperature of 310 K, and two intermediate points, each halfway between the zero displacements and one maximum (see Color Plate 1).

Electrostatic calculations were performed with the programs ESPOT and ESFIELD to determine the electrostatic potential and field as previously described.[29] Distance-dependent Coulombic treatments were applied to the assigned partial atomic charges. Water molecules were excluded from the electrostatic calculations.

GRAPHICAL REPRESENTATIONS

The interactive graphics program Flex (written by M. Pique) was designed to facilitate the visualization of protein flexibility and internal motion. For normal-mode displays, Flex reads a file containing the minimized atomic coordinates and files with the absolute atomic vector displacements for up to six individual, precalculated normal modes. These normal modes can then be displayed both individually and in any selected combination as vibrations whose amplitudes are controlled by interactively adjusting the temperature of the system. Flex achieves this not by precalculating harmonic sinusoidal snapshots, but by computing the resultant atomic displacements as the system is being displayed. Several viewing styles with stereo capability are available, including sticks, ball-and-stick, space-filling CPK spheres, and backbone ribbon.

We have developed two animated computer graphical representations of the changes in the electrostatic field and potential that result from molecular motion. A major advantage of both methods is that, once the data processing has been carried out, the changes can be viewed in real time. The first method employed the programs GRAMPS,[43] which has a richer visual environment than Flex (such as labels and arrows), and GRANNY[44] displayed on an Evans and Sutherland MPS connected to a VAX 11/750. The animation capability of GRAMPS was used to step through a script of snapshots frame by frame. For each of the different displacements, the electrostatic field was calculated with ESFIELD,[29] at points on concentric spheres from the area of interest. As in previous work,[29] the direction of the field at each point was represented as an arrow, generated by ESARROW, and color-coded according to electrostatic potential. Each set of displaced coordinates, together with its corresponding electrostatic field vectors, was entered as a snapshot frame into GRAMPS. The frames could then be displayed sequentially, going from one maximum displacement to the other and back to simulate the motion of the mode, resulting in a smooth motion with five displacements.

The second method applied a recently developed algorithm[45] to generate a consensus surface from several independent surfaces using spherical harmonic approximations. Expanded molecular surfaces of the two maximum displacement structures were calculated using the program MS, applying the Connolly solvent-accessible surface algorithm.[46] A sphere of radius of 1.4 Å was rolled over the individual atoms with their radii enlarged by 6 Å. This created a smooth, expanded surface that followed the contours of the protein surface, but remained 6 Å away from the van der Waals surface. The coordinates for the points forming the two maximum displacement expanded surfaces were combined, and a fifth-order spherical harmonic approximation of a consensus surface was made using the program Sphinx.[45] For each displacement along the normal mode, the electrostatic potential at each point on the consensus surface was determined using ESPOT and the points were color coded using the program ESSURF.[29] With the program Vu, the α-carbon backbones of the displacement structures were displayed sequentially on the Stardent 1520, together with the fixed points of the consensus surface color coded electrostatically to correspond to the appropriate displacement. As the protein moved, the fixed surface points changed color. Vu, developed by Matthew Fitzgibbon of the University of North Carolina, Chapel Hill, simultaneously or sequentially reads and displays files containing sets of x, y, and z coordinates and associated colors for dots and lines.

RESULTS

Two hundred normal modes, with wavenumbers ranging from about 50 to 1 cm^{-1}, corresponding to vibration times of about 1×10^{-12} to 3×10^{-11} s $cycle^{-1}$ (from the relationship frequency = speed of light × wavenumber) were obtained from AMBER for the superoxide dismutase monomer. Fast vibration times (<1 ns) of charged atoms prevent complete solvent and counterion screening.[47] Therefore, at normal-mode frequencies, charges will not be efficiently damped and long-range electrostatic interactions are expected to be important. For SOD, the 20 normal-mode frequencies that had the largest movements in residues Thr 56, Glu 130, Glu 131, Lys 134, Thr 135, and Arg 141, which lie around the rim of the active site channel (see Figure 1), were chosen for a more focused analysis. To analyze potential effects on long-range electrostatic recognition, each mode was examined individually with Flex, to characterize the type of motion around the active site channel, whether a concerted rocking, twisting, or opening-and-closing, etc., that was occurring. The lowest frequency modes were of greater interest, because of their longer time scales and more global motions. The vibrational mode chosen as an example for developing graphics methods had a frequency of 9.8 cm^{-1}, corresponding to an energy of 0.028 kcal mol^{-1} and a vibration time of about 3×10^{-12} s $cycle^{-1}$. This mode exhibited an opening-and-closing motion around the active site due to the swinging of the overhanging loop containing Glu 130, Glu 131, and Lys 134, residues believed to be important in the electrostatic guidance of the anionic superoxide substrate into the active site.[29] The movement of this loop relative to the rest of the molecule can be seen in the larger RMS deviations for the loop residues in the displaced structure generated from this mode (Figure 2).

The five sample displacements for the mode (described above) were then calculated assuming a physiological temperature of 310 K (37 °C). The average RMS displacement

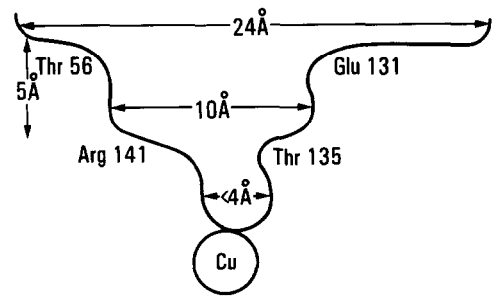

Figure 1. A schematic view of the active site channel of superoxide dismutase in cross section. The amino acids that form the channel and its shape and dimensions are indicated

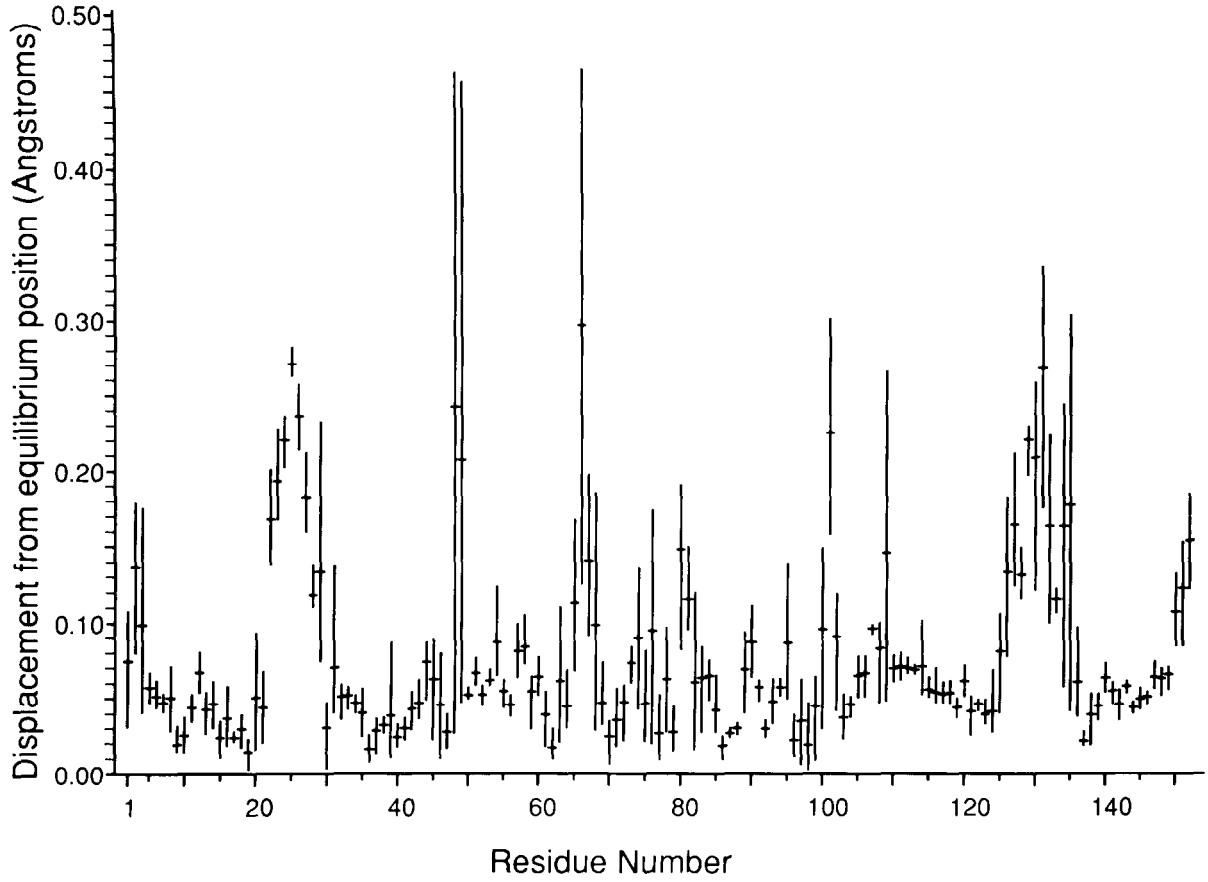

Figure 2. Atomic displacements from equilibrium positions for the superoxide dismutase normal mode at 9.8 cm^{-1}. The upper and lower limits of the bar at each residue number show the maximum and minimum movement for any of the residue's heavy atoms, and the tick mark shows the overall RMS deviation for the heavy atoms of the residue

from the energy-minimized structure to the extreme position of the model was 0.16 Å for the heavy atoms of the six residues listed above, as compared with 0.10 Å for all the heavy atoms in the structure (see Figure 2). Of the six residues, Glu 130 moved the most, with an average RMS deviation of 0.28 Å for all heavy atoms in the residue. (The maximum displacement for any atom of Glu 130 was 0.35 Å for the carboxyl carbon.) Arg 141 moved the least, with an average RMS deviation of 0.06 Å for the residue overall. The electrostatic field vectors for each position were calculated at points lying outside the protein surface on concentric spheres from 0 to 14 Å around the active site, measured from the position of a crystallographically determined water molecule bound to the copper ion at the bottom of the active site channel (such as the vectors shown in Color Plate 2). The five frames were displayed and animated using GRAMPS[43] and GRANNY,[44] so the effect of the motion could be easily visualized.

Two prominent features of the mode at 9.8 cm^{-1} were seen. First, there was a concerted tilting of the field vectors into and out of the channel above the active site, as the protein moved from one extreme of the normal mode to the other. This arose from the concerted movement of the charged groups on the outer rim across and down toward the active site, then out and away, somewhat like jaws opening and closing. Second, the field focused just above the open copper site near the Arg 141 side chain became more positive as the Glu 131 moved away from the channel. The resultant average change in the direction of the electrostatic field vectors was 5.4°, with a maximum angular difference of 25.0°. Larger differences in the vector directions were observed when several modes were combined assuming the phases of the modes interfered constructively (see Color Plate 2).

The consensus surface was derived from the expanded molecular surfaces of the two maximal displacements. For each of the five sets of coordinate displacements, the electrostatic potential at each point of the consensus surface was then calculated and color coded. The complete surface for the minimized position is shown in Color Plate 3. The Cα chain was displayed simultaneously to facilitate the correlation of molecular motion with changes in the surrounding electrostatic potential. The resultant frames were cycled through using the program Vu. The positive patches over the active site for the two extreme displacements are shown in Color Plate 4. The surface points remain fixed in position, but change color as the protein moves. Patches of charge in the dimer interface did not move much with this particular mode. The positive patch over the active site, however, moved back and forth above the channel.

CONCLUSIONS

We have presented two new and complementary approaches for evaluating the effect of protein flexibility on the surrounding electrostatic environment. The animation of field vectors based upon predetermined protein movement is primarily useful for detailed examinations of a specific locality, such as an enzyme's active site. The complementary approach of animating electrostatic potentials by color coding on expanded spherical harmonic surfaces provides a more global view. The changes in electrostatic potential, as viewed on a fixed spherically harmonic consensus surface, give an easily comprehensible representation for an entire protein. Neither of these visualizations of molecular flexibility effects are limited to the display of changes in electrostatic properties due to normal mode motions, but are equally applicable for displaying changes in any chemical or molecular property due to any defined set of protein movements.

In developing these new computer graphics methods, we have made several approximations that may have resulted in an underestimation of the effects of normal-mode motion on the electrostatics. First, we have focused on only one mode (Color Plate 1), rather than looking at a combination of all of the modes or at least a large subset of them. Combining modes will result in cases where the motions interfere constructively, amplifying particular movements at certain times (see Color Plate 2). Second, we have heavily dispersed the charges of the copper and zinc ions throughout their ligands (Table 2), in effect exaggerating the delocalization of the highly positive charges at the active site. Finally, we have minimized the protein as a virtually isolated system, without solvent to counteract the Coulombic attraction between unlike charges. Consequently, the charged side chains on the surface of the enzyme have tended to collapse inward, damping the effect of the charges on the electrostatic surface. To date, normal-mode calculations have focused on small proteins, such as bovine pancreatic trypsin inhibitor.[48,49] Although we have applied this approach to a much more complex protein, the inclusion of bulk solvent still remains a significant problem that must be addressed.

Despite these necessary approximations, application of these visualization methods to SOD suggest that modeling molecular motions may be important for studies of molecular recognition and interactions in two respects. Although small, the movements within the diameter of the active site are potentially significant when considering the time scale that it takes for a superoxide molecule to move into the channel from about 15 Å away. Moreover, all of these movements occur at frequencies above the expected threshold frequency for long-range electrostatic interactions.[47] The observed vibrational frequencies should reduce the screening effect of solvent so that it may actually be correctly modeled as a dielectric medium, which has previously proved useful for SOD,[29] and is consistent with new experimental results on mutant SODs (J. Tainer, R. Hallewell, D. Cabelli, and E. Getzoff, unpublished results).

Whether or not normal-mode analysis proves ideal for examining protein interactions, the local and global flexibility of macromolecules is undoubtedly a functionally important property that should be included in molecular visualization and analysis. The two new molecular computer graphics approaches we have developed and applied to SOD should facilitate future work in this area.

ACKNOWLEDGMENTS

We gratefully acknowledge David A. Case for assistance in carrying out the normal-mode calculations and Gary H. Liao for assistance with graphics and programming. This work was supported by NIH Fellowship GM11612 (CLF), ONR N00014-89-J-1174 (EDG), NIH R01 GM39345 (JAT), and NSF 8822385 (EDG, JAT, and MEP).

REFERENCES

1 Rogers, N. K. The modelling of electrostatic interactions in the function of globular proteins. *Prog. Biophys. Mol. Biol.* 1986, **48**, 37–66
2 Mauk, M. R., Mauk, A. G., Weber, P. C. and Matthew, J. B. Electrostatic analysis of the interaction of cytochrome *c* with native and dimethyl ester heme substituted cytochrome b_5. *Biochemistry* 1986, **25**, 7085–7091
3 Wendoloski, J. J., Matthew, J. B., Weber, P. C. and Salemme, F. R. Molecular dynamics of a cytochrome c-cytochrome b_5 electron transfer complex. *Science* 1987, **238**, 794–797
4 Cheddar, G., Meyer, T. E., Cusanovich, M. A., Stout, C. D. and Tollin, G. Electron-transfer reactions between flavodoxin semiquinone and *c*-type cytochromes: comparisons between various flavodoxins. *Biochemistry* 1986, **25**, 6502–6507
5 Hazzard, J. T., McLendon, G., Cusanovich, M. A. and Tollin, G. Formation of electrostatically-stabilized complex at low ionic strength inhibits interprotein electron transfer between yeast cytochrome *c* and cytochrome *c* peroxidase. *Biochem. Biophys. Res. Commun.* 1988, **151**, 429–434
6 Bernhardt, R., Kraft, R., Otto, A. and Ruckpaul, K. Electrostatic interactions between cytochrome P-450 LM2 and NADPH-cytochrome P-450 reductase. *Biomed. Biochim. Acta* 1988, **47**, 581–592
7 Rush, J. D. and Koppenol, W. H. Electrostatic interactions of 4-carboxy-2,6-dinitrophenyllysine-modified cytochromes *c* with physiological and non-physiological redox partners. *Biochim. Biophys. Acta* 1988, **936**, 187–198
8 Stewart, D. E., LeGall, J., Moura, I., Moura, J. J., Peck, Jr., H. D., Xavier, A. V., Weiner, P. K. and Wampler, J. E. A hypothetical model of the flavodoxin-tetraheme cytochrome c3 complex of sulfate-reducing bacteria. *Biochemistry* 1988, **27**, 2444–2450
9 Nadler, S. G. and Strobel, H. W. Role of electrostatic interactions in the reaction of NADPH-cytochrome P-450 reductase with cytochromes P-450. *Arch. Biochem. Biophys.* 1988, **261**, 418–429
10 Takabe, T., Takenaka, K., Kawamura, H. and Beppu, Y. Charges on proteins and distances of electron transfer in metalloprotein redox reactions. *J. Biochem.* 1986, **99**, 833–890
11 Churg, A. K. and Warshel, A. Control of the redox

potential of cytochrome *c* and microscopic dielectric effects in proteins. *Biochemistry* 1986, **25**, 1675–1681
12 Mrabet, N. T., McDonald, M. J., Turci, S., Sarkar, R., Szabo, A. and Bunn, H. F. Electrostatic attraction governs the dimer assembly of human hemoglobin. *J. Biol. Chem.* 1986, **261**, 5222–5228
13 Warshel, A., Naray-Szabo, G., Sussman, F. and Hwang, J. K. How do serine proteases really work? *Biochemistry* 1989, **28**, 3629–3637
14 Akahane, K. and Umeyama, H. Binding specificity of papain and cathepsin b. *Enzyme* 1986, **36**, 141–149
15 Carlson, W. D., Handschumacher, M., Summers, N., Karplus, M. and Haber, E. Models for the three-dimensional structure of renin inhibitors bound in the active site of human renin: an analysis of the properties that produce tight binding. *J. Cardiovasc. Pharmacol.* 1987, **10**(Suppl. 7), S91–S93
16 Knorre, D. G., Lavrik, O. I. and Nevinsky, G. A. Protein–nucleic acid interaction in reactions catalyzed with DNA polymerases. *Biochimie* 1988, **70**, 655–661
17 Jen-Jacobson, L., Lesser, D. and Kurpiewski, M. The enfolding arms of EcoRI endonuclease: role in DNA binding and cleavage. *Cell* 1986, **45**, 619–629
18 Warwicker, J. Investigating protein–protein interaction surfaces using a reduced stereochemical and electrostatic model. *J. Mol. Biol.* 1989, **206**, 381–395
19 Brooks, C., Pettitt, B. M. and Karplus, M. Proteins: a theoretical perspective of dynamics, structure, and thermodynamics. *Adv. Chem. Phys.* 1987, **71**, 14–21
20 Warshel, A. and Russell, S. T. Calculations of electrostatic interactions in biological systems and in solutions. *Quart. Rev. Biophys.* 1984, **17**, 283–422
21 Harvey, S. C. Treatment of electrostatic effects in macromolecular modeling. *Proteins: Struct. Func. Gen.* 1989, **5**, 78–92
22 Pettitt, B. M. and Karplus, M. Role of electrostatics in the structure, energy, and dynamics of biomolecules: a model study of *N*-methylalanylacetamide. *J. Am. Chem. Soc.* 1985, **107**, 1166–1173
23 Cudd, A. and Fridovich, I. Electrostatic interactions in the reaction mechanism of bovine erythrocyte superoxide dismutase. *J. Biol. Chem.* 1982, **257**, 11443–11447
24 Argese, E., Viglino, P., Rotilio, G., Scarpa, M. and Rigo, A. Electrostatic control of the rate-determining step of the copper, zinc superoxide dismutase catalytic reaction. *Biochemistry* 1987, **26**, 3224–3228
25 Tainer, J. A., Getzoff, E. D., Richardson, J. S. and Richardson, D. C. Structure and mechanism of copper, zinc superoxide dismutase. *Nature* 1983, **306**, 284–287
26 Hodgson, E. K. and Fridovich, I. The interaction of bovine erythrocyte superoxide dismutase with hydrogen peroxide: inactivation of the enzyme. *Biochemistry* 1975, **14**, 5294–5303
27 Koppenol, W. H. *The Physiological Role of the Charge Distribution on Superoxide Dismutase*. Academic, New York, 1981, pp. 671–674
28 Koppenol, W. H. *On the Reactivity of the Superoxide Anion and the Biological Function of Superoxide Dismutase*. Pergamon, Oxford, 1982, pp. 127–136
29 Getzoff, E. D., Tainer, J. A., Weiner, P. K., Kollman, P. A., Richardson, J. S. and Richardson, D. C. Electrostatic recognition between superoxide and copper, zinc superoxide dismutase. *Nature* 1983, **306**, 287–290
30 Klug, D., Rabani, J. and Fridovich, I. A direct demonstration of the catalytic action of superoxide dismutase through the use of pulse radiolysis. *J. Biol. Chem.* 1972, **247**, 4839–4842
31 Tainer, J. A., Getzoff, E. D., Richardson, J. S. and Richardson, D. C. 2SOD: Cu,Zn superoxide dismutase complete atomic coordinates (D. C. Richardson and J. S. Richardson) Brookhaven Protein Structure Data Bank, 1980.
32 Tainer, J. A., Getzoff, E. D., Beem, K. M., Richardson, J. S. and Richardson, D. C. Determination and analysis of the 2 Å structure of copper, zinc superoxide dismutase. *J. Mol. Biol.* 1982, **160**, 181–217
33 Klapper, I., Hagstrom, R., Fine, R., Sharp, K. and Honig, B. Focusing of electric fields in the active site of Cu-Zn superoxide dismutase: effects of ionic strength and amino-acid modification. *Proteins: Struct. Funct. Gen.* 1986, **1**, 47–59
34 Sharp, K., Fine, R. and Honig, B. Computer simulations of the diffusion of a substrate to an active site of an enzyme. *Science* 1987, **236**, 1460–1463
35 Allison, S. A., Ganti, G. and McCammon, J. A. Simulation of the diffusion-controlled reaction between superoxide and superoxide dismutase, I. Simple models. *Biopolymers* 1985, **24**, 1323–1336
36 Allison, S. A., Northrup, S. H. and McCammon, J. A. Extended Brownian dynamics of diffusion controlled reactions. *J. Chem. Phys.* 1985, **83**, 2894–2899
37 Allison, S. A. and McCammon, J. A. Dynamics of substrate binding to copper zinc superoxide dismutase. *J. Phys. Chem.* 1985, **89**, 1072–1074
38 Allison, S. A., Northrup, S. H. and McCammon, J. A. Simulation of biomolecular diffusion and complex formation. *Biophys. J.* 1986, **49**, 167–175
39 Ganti, G., McCammon, J. A. and Allison, S. A. Brownian dynamics of diffusion-controlled reactions: the lattice method. *J. Phys. Chem.* 1985, **89**, 3899–3902
40 Allison, S. A., Bacquet, R. J. and McCammon, J. A. Simulation of the diffusion controlled reaction between superoxide and superoxide dismutase, II. Detailed models. *Biopolymers* 1987, **27**, 251–269
41 Weiner, P. K. and Kollman, P. A. AMBER: assisted model building with energy refinement. A general program for modeling molecules and their interactions. *J. Comput. Chem.* 1981, **2**, 287–303
42 Weiner, S. J., Kollman, P. A., Case, D. A., Singh, U. C., Ghio, C., Alagona, G., Profeta, Jr., S. and Weiner, P. A new force field for molecular mechanical simulation of nucleic acids and proteins. *J. Am. Chem. Soc.* 1984, **106**, 765–784
43 O'Donnell, T. J. and Olson, A. J. GRAMPS—A graphics language interpreter for real-time, interactive, three-dimensional picture editing and animation. *Comput. Graphics* 1981, **15**, 133–142
44 Connolly, M. L. and Olson, A. J. GRANNY, a companion to GRAMPS for the real-time manipulation of macromolecular models. *Comput. Chem.* 1985, **9**, 1–6
45 Max, N. L. and Getzoff, E. D. Spherical harmonic molecular surfaces. *IEEE Comput. Graphics Appl.* 1988, **8**, 42–50

46 Connolly, M. L. Solvent-accessible surfaces of proteins and nucleic acids. *Science* 1983, **221**, 709–713
47 Grigera, J. R., Vericat, F., Ruderman, G. and de Xammar Oro, J. R. On the threshold frequency of long-range interactions in physiological solutions. *Chem. Phys. Lett.* 1989, **156**, 615–618
48 Brooks, B. and Karplus, M. Harmonic dynamics of proteins: normal modes and fluctuations in bovine pancreatic trypsin inhibitor. *Proc. Natl. Acad. Sci. USA* 1983, **80**, 6571–6575
49 Nishikawa, T. and Go, N. Normal modes of vibration in bovine pancreatic trypsin inhibitor and its mechanical property. *Proteins: Struct. Func. Gen.* 1987, **2**, 308–329